

Many-body theory of gamma spectra from positron–atom annihilation

L J M Dunlop and G F Gribakin

Department of Applied Mathematics and Theoretical Physics, Queen's University,
Belfast BT7 1NN, UK

E-mail: l.dunlop@qub.ac.uk and g.gribakin@qub.ac.uk

Received 15 December 2005, in final form 16 December 2005

Published 13 March 2006

Online at stacks.iop.org/JPhysB/39/1647

Abstract

A many-body theory approach to the calculation of gamma spectra of positron annihilation on many-electron atoms is developed. We evaluate the first-order correlation correction to the annihilation vertex and perform numerical calculations for the noble gas atoms. Extrapolation with respect to the maximal orbital momentum of the intermediate electron and positron states is used to achieve convergence. The inclusion of correlation corrections improves agreement with experimental gamma spectra.

(Some figures in this article are in colour only in the electronic version)

1. Introduction

The main aim of our paper is to develop a many-body theory approach to the calculation of gamma spectra from positron–atom annihilation.

Positron annihilation has been an important tool for studying electronic and atomic structures of solids for over half a century. Its history can be traced from the first review of the theory of positron annihilation in solids by Ferrel (1956) to a more recent work by Puska and Nieminen (1994). Positron lifetimes and spectra of annihilation gamma quanta contain information about the structure and composition of bulk materials and surfaces, presence and concentration of defects and voids or pores, and their sizes, and electron momentum distribution. Interpretation of positron annihilation data requires good theoretical understanding of the process. Many-body theory was the first method used to determine positron annihilation rates in metals (Kahana 1963, Carbotte 1967). In particular, it was successful in explaining large enhancement factors that increase the annihilation rates above that obtained in the noninteracting electron gas approximation (see also Arponen and Pajanne (1979)).

In the 1990s measurements of gamma-ray spectra from positron annihilation on atoms and molecules in the gas phase became possible (Tang *et al* 1992, Coleman *et al* 1994).

For He the experiment showed excellent agreement with the calculated spectrum obtained from an elaborate variational positron–He wavefunction (Van Reeth *et al* 1996). This work also revealed sizeable deviations of the spectrum from a Gaussian, which is often used as an approximation. For noble gas atoms of Ar, Kr and Xe, a careful study of the shape of the 511 keV gamma-ray line provided an estimate of the contribution of positron annihilation with inner-shell electrons (Iwata *et al* 1997b). A large systematic study was conducted for a variety of inorganic molecules, alkanes, alkenes, aromatics and perfluorinated and partially fluorinated hydrocarbons (Iwata *et al* 1997a). In particular, this work determined the relative probability of annihilation on the fluorine atoms and on the C–H bonds for partially fluorinated hydrocarbons. Such information is important for achieving better understanding of very large positron annihilation rates on polyatomic molecules (see, e.g., Surko *et al* (2005)).

On the theory side, much progress in understanding the interaction of low-energy positrons with many-electron atoms has been obtained by using many-body theory. Its application to positron–atom collisions was pioneered by Amusia *et al* (1976) who considered positron scattering from He. Subsequently, the effect of virtual positronium (Ps) formation on positron–atom interaction was investigated for heavier noble gas atoms (Dzuba *et al* 1993, 1996). These works showed that virtual Ps formation gives a large contribution to the positron–atom attraction¹. It leads to the emergence of positron–atom virtual and bound states (Dzuba *et al* 1995, 1996), and completely alters the picture of low-energy positron–atom scattering (Gribakin and King 1996). These papers employed an approximate method of accounting for virtual Ps formation. Recently, a consistent many-body theory approach has been developed. It is based on the summation of the electron–positron ladder diagram series (Ludlow 2003, Gribakin and Ludlow 2004). Its contribution is especially important for the calculation of the annihilation rate. These and earlier calculations (Dzuba *et al* 1993, 1996) have demonstrated that electron–positron correlation effects can enhance the positron–atom annihilation rate as much as 10^3 times.

In the paper by Iwata *et al* (1997b), the fraction of annihilation with inner-shell electrons was derived by fitting the experimental data with a linear combination of the gamma spectra for the valence and inner shells. These spectra were calculated in the simplest approximation, by using the positron wavefunction in the static field of the atom. In spite of a complete neglect of electron–positron correlations, the shapes of the measured gamma spectra were described reasonably well. On the other hand, some discrepancies between the theoretical and experimental spectra were obvious, adding uncertainty to the estimates of the inner-shell annihilation fractions. For example, the data for Ar were compatible with a zero contribution of annihilation with 2s and 2p electrons.

Since correlation effects play such a large role in positron–atom interactions, they must be included in the proper theory of annihilation gamma spectra. In what follows, we briefly recount the main facts and formulae concerning positron annihilation and gamma spectra using the formalism of creation–destruction operators (section 2). We then proceed to derive the many-body diagrammatic expansion of the annihilation amplitude, and consider the significance of various terms and their relation to the total annihilation rate (section 3). In section 4, expressions for the zeroth- and first-order contributions are reduced to products of radial matrix elements, which can be evaluated numerically. Section 5 reports the results of such calculations for the noble gas atoms, which confirm that the correlation corrections to the annihilation amplitude have a marked effect on the gamma spectra. We also demonstrate the

¹ This explained the success of earlier polarized-orbital calculations in describing positron elastic scattering and annihilation for noble gas atoms (McEachran *et al* 1980 and references therein). In that approximation, the positron was treated as a heavy particle, and the strength of the positron–atom polarization potential was overestimated, making up for the complete neglect of virtual Ps formation.

importance of extrapolation over the maximal orbital angular momentum of the intermediate electron and positron states. In the appendix, expressions for the annihilation amplitudes involving many-particle wavefunctions in coordinate space are given.

2. Basic theory

2.1. Annihilation operator

Due to the conservation of momentum, annihilation of an electron–positron pair must lead to the emission of at least two photons². In fact, according to quantum electrodynamics (QED), annihilation into two photons is possible only if the total spin S of the pair is zero (Berestetskii *et al* 1982). For $S = 1$ the annihilation results in the emission of three photons³.

In QED the process of electron–positron annihilation is described by the second- or third-order diagram, depending on the number of photons emitted (Berestetskii *et al* 1982). The photons carry away the energy of the particles, $\sim 2mc^2$, and have large momenta $\sim mc$, where m is the electron mass, and c is the speed of light. Intermediate electron/positron states in the QED diagrams have similar momenta. They are much larger than the typical momenta of valence and inner-shell atomic electrons (with the exception of 1s electrons in heavy atoms with $Z \sim 100$), or the positron momentum in a typical experiment⁴. As a result, the annihilation amplitude is independent of the electron and positron momenta. Hence, the *effective operator* for annihilation into gamma quanta with the total momentum \mathbf{P} is proportional to

$$\sum_{\mathbf{k}_1, \mathbf{k}_2} \hat{a}_{\mathbf{k}_1} \hat{b}_{\mathbf{k}_2} \delta_{\mathbf{k}_1 + \mathbf{k}_2, \mathbf{P}}, \quad (1)$$

where $\hat{a}_{\mathbf{k}_1}$ ($\hat{b}_{\mathbf{k}_2}$) is the destruction operator of the electron (positron) with momentum \mathbf{k}_1 (\mathbf{k}_2), and the δ -function ensures momentum conservation, $\mathbf{P} = \mathbf{k}_1 + \mathbf{k}_2$ (Ferrell 1956). Using electron and positron destruction operators $\hat{\psi}(\mathbf{r})$ and $\hat{\phi}(\mathbf{r})$ in the coordinate representation

$$\hat{a}_{\mathbf{k}} = \frac{1}{\sqrt{V}} \int e^{-i\mathbf{k}\cdot\mathbf{r}} \hat{\psi}(\mathbf{r}) \, d\mathbf{r}, \quad (2)$$

$$\hat{b}_{\mathbf{k}} = \frac{1}{\sqrt{V}} \int e^{-i\mathbf{k}\cdot\mathbf{r}} \hat{\phi}(\mathbf{r}) \, d\mathbf{r}, \quad (3)$$

where V is the normalization volume, the annihilation operator (1) can be re-written as (Ferrell 1956, Chang 1957)

$$\hat{O}_a(\mathbf{P}) \equiv \int e^{-i\mathbf{P}\cdot\mathbf{r}} \hat{\psi}(\mathbf{r}) \hat{\phi}(\mathbf{r}) \, d\mathbf{r}. \quad (4)$$

This equation shows that the annihilation of a *nonrelativistic* electron–positron pair occurs when the particles are at the same point. Physically, this can be explained using the uncertainty principle. Indeed, the spatial separation between the points where the photons are produced is about \hbar/mc . This is much smaller than the Bohr radius $a_0 = \hbar^2/me^2$, i.e. the typical atomic size, or the de Broglie wavelength of the particles involved ($c = 137$ in atomic units, where $\hbar = m = |e| = 1$).

² When this process occurs in an external field, e.g., when the electron is bound in an atom, annihilation into a single quantum is also possible. However, its probability is small; see, e.g., Johnson *et al* (1964).

³ For $S = 0$ annihilation into 2, 4, ... photons is possible, while for $S = 1$ the number of photons must be odd (3, 5, ...). In both cases the process with the smallest number of photons dominates.

⁴ In positron annihilation with matter, even if the initial positron is fast, it quickly loses energy due to inelastic ionizing collisions, and most of the annihilation events involve slow positrons.

In equations (1) and (4) electron and positron spin indices have been suppressed. The operator can be used in this form if the total spin of the electron subsystem is zero. In this case the annihilation rate is equal to that averaged over the positron spin. The rate of annihilation into photons with the total momentum \mathbf{P} is given by the squared modulus of the transition amplitude of operator (4). The total annihilation rate is obtained by integration over $d^3P/(2\pi)^3$ and summation over the final states of the system. The correct absolute magnitude of the 2-photon and 3-photon annihilation rates can be determined by comparison with the spin-averaged positronium annihilation rates (Berestetskii *et al* 1982). In the first case, the squared amplitude must be multiplied by $\pi r_0^2 c$, while in the second case—by $[4(\pi^2 - 9)/3]r_0^2 \alpha c$, where $r_0 = e^2/mc^2$ is the classical electron radius, and $\alpha = e^2/\hbar c$ is the fine structure constant. This shows that 3-photon annihilation is about 10^3 times slower than 2-photon annihilation, and can often be neglected.

2.2. Spectrum of photons and annihilation rates

Let $|i\rangle$ be the state of N electrons and the positron before the annihilation, and $|f\rangle$ —the state of $(N - 1)$ electrons after the annihilation. In two-photon annihilation, the momentum distribution of the photons,

$$W_f(\mathbf{P}) = \pi r_0^2 c |\langle f | \hat{O}_a(\mathbf{P}) | i \rangle|^2, \quad (5)$$

determines their energy spectrum. The total energy of the two photons is

$$E_{\gamma 1} + E_{\gamma 2} = 2mc^2 + E_i - E_f, \quad (6)$$

where E_i and E_f are the energies of the initial and final states (not including the rest energy of the constituent particles), and total photon momentum is $\mathbf{p}_{\gamma 1} + \mathbf{p}_{\gamma 2} = \mathbf{P}$.

For $\mathbf{P} = 0$ the photons are emitted in the opposite direction, $\mathbf{p}_{\gamma 1} = -\mathbf{p}_{\gamma 2}$, and have equal energies, $E_{\gamma 1} = E_{\gamma 2} = mc^2 + \frac{1}{2}(E_i - E_f) \equiv E_\gamma$. For $\mathbf{P} \neq 0$ the photon energy is Doppler shifted, e.g., for the first photon $E_{\gamma 1} = E_\gamma + Vmc \cos \theta$, where $\mathbf{V} = \mathbf{P}/2m$ is the centre-of-mass velocity of the electron-positron pair, θ is the angle between the direction of the photon and \mathbf{V} , and we assume that $V \ll c$ and $p_{\gamma 1} = E_{\gamma 1}/c \approx mc$. Hence, the shift of the photon energy from the centre of the line, $\epsilon = E_{\gamma 1} - E_\gamma$, is

$$\epsilon = \frac{Pc}{2} \cos \theta, \quad (7)$$

and the photon energy spectrum is given by

$$w(\epsilon) = \int W_f(\mathbf{P}) \delta\left(\epsilon - \frac{1}{2}Pc \cos \theta\right) \frac{d^3P}{(2\pi)^3}. \quad (8)$$

Using polar coordinates and averaging over the direction of emission of the photon, one obtains

$$w(\epsilon) = \frac{1}{c} \int \int_{2|\epsilon|/c}^{\infty} W_f(\mathbf{P}) \frac{P dP d\Omega_{\mathbf{P}}}{(2\pi)^3}. \quad (9)$$

On the other hand, using Cartesian coordinates and choosing the z -axis along the direction of the photon, one obtains from (8)

$$w(\epsilon) = \frac{2}{c} \iint W_f(P_x, P_y, 2\epsilon/c) \frac{dP_x dP_y}{(2\pi)^3}. \quad (10)$$

This form shows that the energy spectrum is proportional to the probability density for a component of the momentum \mathbf{P} . Equation (10) allows one to link $w(\epsilon)$ to the quantity measured by the angular correlation of annihilation radiation (ACAR) technique. In ACAR one measures the small angle Θ between the direction of one photon and the plane containing

the other photon⁵. If the direction perpendicular to the plane is x , then $\Theta = P_x/mc$. Given that the distributions of P_x , P_y and P_z are identical (in an isotropic system), one obtains the distribution of Θ from $w(\epsilon)$ by a simple change of variable, $\Theta = 2\epsilon/mc^2$.

When a low-energy positron annihilates with a bound electron whose energy is ϵ_n , the centre of the photon spectrum is shifted by $\epsilon_n/2$ relative to mc^2 . The width of the two-photon momentum distribution is determined by the typical momenta of the bound electron, $P \sim (2m|\epsilon_n|)^{1/2}$. The corresponding Doppler width of the annihilation spectrum, $\epsilon \sim Pc \sim (|\epsilon_n|mc^2)^{1/2}$, is much greater than its shift. Hence, one can regard the line as centred on $E_\gamma = mc^2 = 511$ keV, even for the annihilation on inner-shell electrons.

The total annihilation rate in the state $|i\rangle$ is obtained by integration over the momentum \mathbf{P} and summation over the final states

$$\begin{aligned}\lambda &= \sum_f \int W_f(\mathbf{P}) \frac{d^3 P}{(2\pi)^3} \\ &= \pi r_0^2 c \sum_f \int \langle i | \hat{O}_a^\dagger(\mathbf{P}) | f \rangle \langle f | \hat{O}_a(\mathbf{P}) | i \rangle \frac{d^3 P}{(2\pi)^3}.\end{aligned}\quad (11)$$

Using closure in the subspace of $(N-1)$ -electron states, $\sum_f |f\rangle\langle f| = 1$, substituting (4) and integrating over \mathbf{P} , we have

$$\lambda = \pi r_0^2 c \int \langle i | \hat{n}_-(\mathbf{r}) \hat{n}_+(\mathbf{r}) | i \rangle d\mathbf{r}, \quad (12)$$

where $\hat{n}_-(\mathbf{r}) = \hat{\psi}^\dagger(\mathbf{r})\hat{\psi}(\mathbf{r})$ and $\hat{n}_+(\mathbf{r}) = \hat{\phi}^\dagger(\mathbf{r})\hat{\phi}(\mathbf{r})$ are the electron and positron density operators. The annihilation rate is thus given by the expectation value of the electron density at the positron integrated over the positron coordinates.

Equation (12) gives the two-photon annihilation rate for a bound positron–atom state $|i\rangle$. The annihilation rate for a positive-energy positron moving through a gas of atoms is given by a similar formula (Fraser 1968)

$$\lambda = \pi r_0^2 c n Z_{\text{eff}}, \quad (13)$$

where n is the number density of the gas, and

$$Z_{\text{eff}} = \int \langle i | \hat{n}_-(\mathbf{r}) \hat{n}_+(\mathbf{r}) | i \rangle d\mathbf{r}. \quad (14)$$

Here the state $|i\rangle$ describes a collision between the positron with momentum \mathbf{k} and the atom (usually in the ground state). It is normalized to the positron plane wave $e^{i\mathbf{k}\cdot\mathbf{r}}$ at large positron–atom separations, i.e., to one positron per unit volume. The dimensionless parameter Z_{eff} is interpreted as the *effective number* of target electrons which contribute to the annihilation.

If one neglects the interaction between the positron and the atom and writes the initial state as $|i\rangle = \sqrt{V} b_{\mathbf{k}}^\dagger |0\rangle$, where $|0\rangle$ is the ground state of the N -electron atom, equation (14) gives $Z_{\text{eff}} = N$. In reality, the values of Z_{eff} can be very different from the actual number of electrons (see, e.g., Surko *et al* (2005)). Repulsion from the nucleus prevents the positron from penetrating into the atom, suppressing the probability of its annihilation with the inner electrons. On the other hand, the long-range positron–atom attraction increases the positron density near the atom, making Z_{eff} larger. The Coulomb attraction within the annihilating electron–positron pair increases Z_{eff} further (Dzuba *et al* 1996, Gribakin and Ludlow 2004).

⁵ This is so-called 1D-ACAR. A more advanced technique, 2D-ACAR, involves measuring the angle between the directions of the photons, i.e. *two* projections of the momentum. The corresponding distribution is proportional to $\int W_f(P_x, P_y, P_z) dP_z$, and is useful for studying the electron density and momentum distribution in anisotropic systems, e.g., solids (Puska and Nieminen 1994).

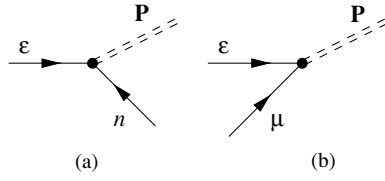


Figure 1. Annihilation amplitude for a positron in state ε and electron in state n occupied in the atomic ground state (a), or an excited electron in state μ (b). The double dashed line corresponds to the annihilation gamma quanta with momentum \mathbf{P} .

Note that the rate (13) is related to the positron–atom annihilation cross section σ_a by $\lambda = \sigma_a n v$, where v is the incident positron velocity, so that $\sigma_a = \pi r_0^2 Z_{\text{eff}}^2 c/v$. On the other hand, equation (14) shows that Z_{eff} has the form of a transition amplitude between two identical states $|i\rangle$. Hence, a perturbation series expansion for this quantity can be developed (Dzuba *et al* 1993).

3. Many-body theory

3.1. Bases and building blocks

When studying positron–atom interactions by many-body theory methods, it is convenient to use the bases of electron and positron states of the Hartree–Fock Hamiltonian of the ground-state atom. Denoting the corresponding electron (positron) wavefunctions and destruction operators by ψ_μ (φ_ν) and \hat{a}_μ (\hat{b}_ν), respectively, we have

$$\hat{\psi}(\mathbf{r}) = \sum_{\mu} \psi_{\mu}(\mathbf{r}) \hat{a}_{\mu}, \quad \hat{\varphi}(\mathbf{r}) = \sum_{\nu} \varphi_{\nu}(\mathbf{r}) \hat{b}_{\nu}. \quad (15)$$

Substituting into (4) we obtain the effective annihilation operator in the form

$$\hat{O}_a(\mathbf{P}) = \sum_{\mu} \sum_{\nu} \langle \mathbf{P} | \delta | \mu \nu \rangle \hat{a}_{\mu} \hat{b}_{\nu}, \quad (16)$$

where

$$\begin{aligned} \langle \mathbf{P} | \delta | \mu \nu \rangle &= \int e^{-i\mathbf{P}\cdot\mathbf{r}} \psi_{\mu}(\mathbf{r}) \varphi_{\nu}(\mathbf{r}) \, d\mathbf{r} \\ &\equiv \int e^{-i\mathbf{P}\cdot(\mathbf{r}_1+\mathbf{r}_2)/2} \delta(\mathbf{r}_1 - \mathbf{r}_2) \psi_{\mu}(\mathbf{r}_1) \varphi_{\nu}(\mathbf{r}_2) \, d\mathbf{r}_1 \, d\mathbf{r}_2. \end{aligned} \quad (17)$$

The second form explains the presence of δ in our notation for the amplitude. Note that the sum over μ in equation (16) contains two distinct contributions, $\sum_{\mu} = \sum_{\mu \leq F} + \sum_{\mu > F}$. The first sum includes the electron states occupied in the atomic ground state, i.e., those at or below the Fermi level F (‘holes’). The corresponding terms in the operator (16) describe positron annihilation which leads to creation of a hole, as shown by diagram (a) in figure 1. The second sum is over the electron states above the Fermi level (‘particles’), and describes positron annihilation with an excited electron, diagram (b) in figure 1.

Substituting (15) and their analogues for $\hat{\psi}^{\dagger}(\mathbf{r})$ and $\hat{\varphi}^{\dagger}(\mathbf{r})$ into $\hat{n}_-(\mathbf{r})$ and $\hat{n}_+(\mathbf{r})$, one obtains the electron–positron contact density operator from equation (12) or (14) in the form

$$\int \hat{n}_-(\mathbf{r}) \hat{n}_+(\mathbf{r}) \, d\mathbf{r} = \sum_{\mu, \mu'} \sum_{\nu, \nu'} \langle \nu' \mu' | \delta | \mu \nu \rangle \hat{a}_{\nu}^{\dagger} \hat{a}_{\mu'}^{\dagger} \hat{a}_{\mu} \hat{a}_{\nu}, \quad (18)$$

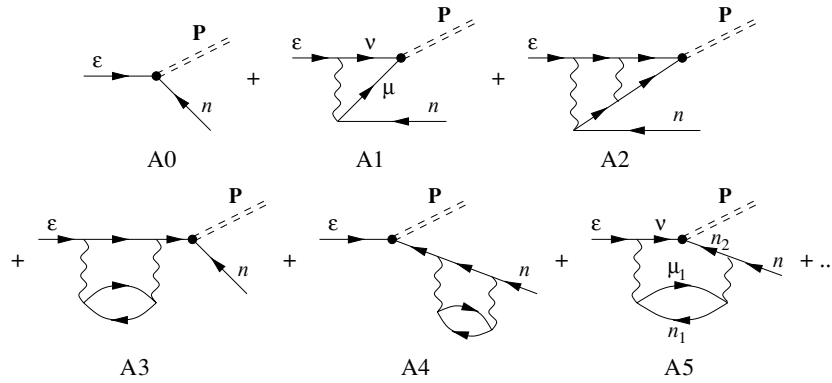


Figure 2. Many-body theory expansion of the positron–atom annihilation amplitude leading to the final state with a hole n . The line starting with ε corresponds to the positron; ν and μ are the intermediate positron and electron states, respectively. Wavy lines correspond to the electron–positron or electron–electron Coulomb interactions.

where μ, μ' and ν, ν' are the electron and positron states, respectively. The amplitude

$$\langle \nu' \mu' | \delta | \mu \nu \rangle = \int \varphi_{\nu'}^*(\mathbf{r}_2) \psi_{\mu'}^*(\mathbf{r}_1) \delta(\mathbf{r}_1 - \mathbf{r}_2) \psi_{\mu}(\mathbf{r}_1) \varphi_{\nu}(\mathbf{r}_2) \mathbf{d}\mathbf{r}_1 \mathbf{d}\mathbf{r}_2 \quad (19)$$

corresponds diagrammatically to a point-like δ vertex with two positron and two electron (particle or hole) lines. It is related to the annihilation amplitude (17) by

$$\langle \nu' \mu' | \delta | \mu \nu \rangle = \int \langle \nu' \mu' | \delta | \mathbf{P} \rangle \frac{d^3 P}{(2\pi)^3} \langle \mathbf{P} | \delta | \mu \nu \rangle. \quad (20)$$

Graphically, this equation is equivalent to connecting the vertices (a) or (b) from figure 1 with their complex conjugates (mirror images) and ‘pulling them together’ by the double-dashed lines, to form a δ vertex with four external lines. This basic relation allows one to relate products of terms in the diagrammatic expansion of the annihilation amplitude $\langle f | \hat{O}_a(\mathbf{P}) | i \rangle$ to the contributions to the total annihilation rate, along the lines of equations (11) and (12) (see below).

3.2. Annihilation amplitudes

Consider a process of two-photon positron annihilation with a ground-state atom

$$e^+ + A \longrightarrow A^+ + 2\gamma. \quad (21)$$

The simplest final state f of the positive ion A^+ is that of an atom with a hole in an electron orbital n . In the lowest order the amplitude of this process is shown by diagram (a), figure 1. The exact amplitude $\langle f | \hat{O}_a(\mathbf{P}) | i \rangle$ can be represented by a many-body theory expansion in powers of the residual electron–positron and electron–electron Coulomb interactions. Figure 2 shows the corresponding zeroth- and first-order diagrams, together with the main types of second-order diagrams.

Analytically, the first diagram in figure 2 is equal to $\langle \mathbf{P} | \delta | n \varepsilon \rangle$ (cf equation (17)). Expressions for the higher order diagrams are constructed using standard atomic many-body theory diagrammatic rules (see, e.g., Amusia and Cherepkov (1975)), modified to account for the *attractive* electron–positron Coulomb interaction. These expressions contain products

of Coulomb and δ -function matrix elements divided by energy denominators. Each energy denominator corresponds to an intermediate state separating two interactions in the diagram. It is given by $E - \sum \varepsilon_{\text{part}} + \sum \varepsilon_{\text{hole}} + i0$, where the sums are over all particles⁶ and all holes in the intermediate state, E is the energy entering the diagram and the infinitesimal imaginary $i0$ defines the way of bypassing the pole. Summation over all intermediate positron and/or electron states is carried out. The overall sign factor for a diagram is given by $(-1)^{N_h + N_l + N_{ep}}$, where N_h , N_l and N_{ep} are the numbers of internal hole lines, electron–hole loops and electron–positron interactions, respectively.

For example, the first-order diagram A1 in figure 2 corresponds to

$$-\sum_{\mu, \nu} \frac{\langle \mathbf{P} | \delta | \mu \nu \rangle \langle \nu \mu | V | n \varepsilon \rangle}{\varepsilon - \varepsilon_\nu - \varepsilon_\mu + \varepsilon_n}, \quad (22)$$

where

$$\langle \nu \mu | V | n \varepsilon \rangle = \int \varphi_\nu^*(\mathbf{r}_2) \psi_\mu^*(\mathbf{r}_1) \frac{1}{|\mathbf{r}_1 - \mathbf{r}_2|} \psi_n(\mathbf{r}_1) \varphi_\varepsilon(\mathbf{r}_2) \mathbf{d}\mathbf{r}_1 \mathbf{d}\mathbf{r}_2 \quad (23)$$

is the Coulomb matrix element. Diagram A1 represents a correction to the annihilation vertex (diagram A0) due to the electron–positron interaction. Note that for low positron energies the denominator in equation (22) is never zero (i.e., the intermediate state is virtual for any ε_ν and ε_μ); hence $i0$ has been dropped.

The second-order diagrams shown in figure 2 have a clear physical interpretation. Thus, diagram A2 represents a higher order correction to the annihilation vertex, similar to diagram A1, with an extra interaction between the annihilating electron and positron. Such contributions are very important because the electron–positron Coulomb attraction strongly enhances the amplitude of finding the two particles at the same point. Diagram A3 describes polarization of the atom by the positron. This polarization gives rise to an attractive positron–atom correlation potential which behaves as $-\alpha_d e^2 / 2r^4$ at large distances, α_d being the atomic dipole polarizability. It has a large effect on the incident positron (see, e.g., Dzuba *et al* (1993, 1996)). Diagram A4 is a correlation correction to the Hartree–Fock wavefunction of the hole. Given that the Hartree–Fock approximation describes atomic ground-state orbitals well, one may expect such corrections to be relatively small. Finally, diagram A5 belongs to another type of vertex corrections in which annihilation takes place in the presence of a virtual hole–particle excitation. We will show below that this and similar diagrams can be neglected because of a specific cancellation between the contributions of certain pairs of diagrams in the photon momentum distribution.

As explained at the end of section 2.2, Z_{eff} can also be presented as a many-body perturbation series. If the state $|i\rangle$ in equation (14) is that of a positron incident on the ground-state atom, Z_{eff} is given by the diagrammatic expansion shown in figure 3. Each of the diagrams contains a δ -function vertex corresponding to the contact density operator (18) with matrix elements (19). The zeroth-order diagram Z0 describes annihilation of the positron with an electron in a Hartree–Fock orbital occupied in the ground state. Its analytical expression,

$$\sum_n \langle \varepsilon n | \delta | n \varepsilon \rangle = \sum_n \int |\psi_n(\mathbf{r})|^2 |\varphi_\varepsilon(\mathbf{r})|^2 \mathbf{d}\mathbf{r}, \quad (24)$$

⁶ If the annihilation photons represented by the double-dashed line are present in the intermediate state, their energy must also be included in $\sum \varepsilon_{\text{part}}$. Since the electron and positron energies do not include their rest energy mc^2 , the energy of the photons must be given with respect to $2mc^2$.

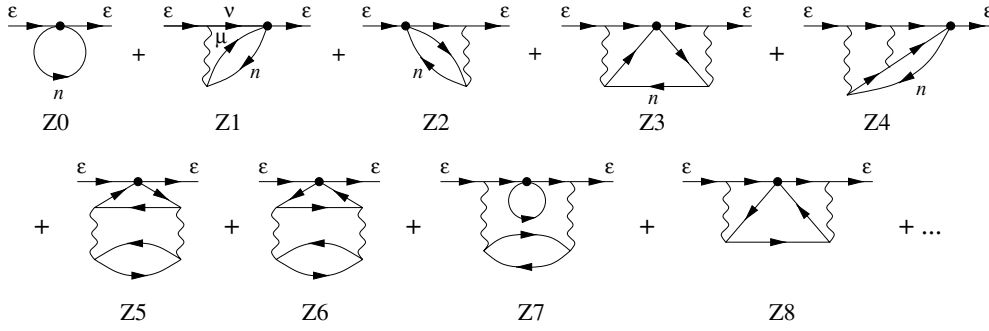


Figure 3. Many-body theory expansion of the positron–atom annihilation rate Z_{eff} . Diagrams Z1–Z8 are corrections to the zeroth-order annihilation vertex, diagram Z0. Corrections to the external positron lines (ε) are not shown.

contains contributions of all occupied electron states n . Higher order diagrams in figure 3 represent correlation corrections to the annihilation vertex. Their analytical expressions are derived using the rules formulated above. For example, diagram Z1 corresponds to

$$-\sum_{\mu, \nu, n} \frac{\langle \varepsilon n | \delta | \mu \nu \rangle \langle \nu \mu | V | n \varepsilon \rangle}{\varepsilon - \varepsilon_\nu - \varepsilon_\mu + \varepsilon_n}, \quad (25)$$

cf equation (22). Note that in figure 3 we do not show corrections to the external positron lines ε , like that in diagram A3 of figure 2. These corrections can be easily included by replacing the positron state φ_ε in the static field of the atom by the positron *Dyson orbital* which accounts for the positron–atom correlation potential (Dzuba *et al* 1996, Gribakin and Ludlow 2004).

By analogy with equations (11)–(12) and (14), the total annihilation rate is related to the momentum distribution of the photon pairs by

$$Z_{\text{eff}} = \sum_f \int |\langle f | \hat{O}_a(\mathbf{P}) | i \rangle|^2 \frac{d^3 P}{(2\pi)^3}. \quad (26)$$

This means that if the terms of the series in figure 2 are multiplied by their complex conjugates and integrated over \mathbf{P} , the expansion for Z_{eff} from figure 3 must be recovered. Indeed, it is easy to see, using equation (20), that the contribution of diagram A0 to the right-hand side of equation (26) (i.e., A0 times its complex conjugate A0*) is equal to diagram Z0, after summation over n . Similarly, the product of diagrams A1 and A0*,

$$\int \langle \varepsilon n | \delta | \mathbf{P} \rangle \frac{d^3 P}{(2\pi)^3} \left[-\sum_{\mu, \nu} \frac{\langle \mathbf{P} | \delta | \mu \nu \rangle \langle \nu \mu | V | n \varepsilon \rangle}{\varepsilon - \varepsilon_\nu - \varepsilon_\mu + \varepsilon_n} \right] = -\sum_{\mu, \nu} \frac{\langle \varepsilon n | \delta | \mu \nu \rangle \langle \nu \mu | V | n \varepsilon \rangle}{\varepsilon - \varepsilon_\nu - \varepsilon_\mu + \varepsilon_n}, \quad (27)$$

gives Z1 (after summation over n), while the product of A1 and A1* becomes Z3.

However, some contributions that appear on the right-hand side of equation (26) do not match any diagrams of the Z_{eff} expansion. In fact, their analytical expressions do not even have the form that would identify them with a particular diagram. For example, consider a product of diagrams A5 and A0* from figure 2

$$\langle \varepsilon n | \delta | \mathbf{P} \rangle \sum_{\nu \mu_1 n_1 n_2} \frac{\langle \mathbf{P} | \delta | n_2 \nu \rangle \langle n_1 n_2 | V | n \mu_1 \rangle \langle \nu \mu_1 | V | n_1 \varepsilon \rangle}{(\varepsilon - \varepsilon_{2\gamma} - \varepsilon_{\mu_1} + \varepsilon_{n_1} + \varepsilon_{n_2})(\varepsilon - \varepsilon_\nu - \varepsilon_{\mu_1} + \varepsilon_{n_1})}, \quad (28)$$

where $\varepsilon_{2\gamma} = \varepsilon + \varepsilon_n$ is the energy of the two gamma quanta with respect to $2mc^2$, given by the energy conservation, $E_{\gamma 1} + E_{\gamma 2} = 2mc^2 + \varepsilon + \varepsilon_n$. It is easy to check that the expression

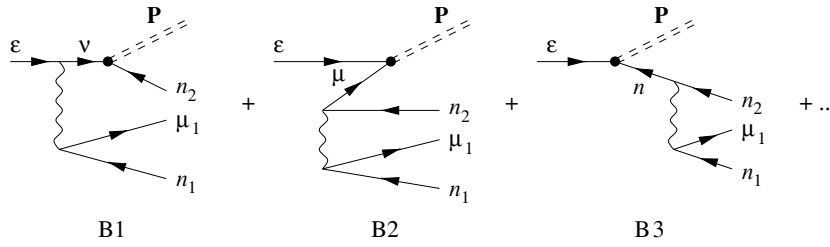


Figure 4. Amplitude of positron annihilation leading to the final state with two holes, n_1 and n_2 , and excited electron μ_1 . For $n_1 \neq n_2$, exchange diagrams with the indices n_1 and n_2 swapped and an extra factor of -1 must also be considered.

obtained upon integration of (28) over \mathbf{P} cannot be drawn as a diagram consistent with the diagrammatic rules. Hence, it also does not correspond to *any* diagram in the expansion of Z_{eff} .

To solve this paradox, note that equation (26) contains a sum over *all* final states. Thus, besides the process shown in figure 2, where positron annihilation leads to a single-hole state, one must consider processes with other types of final states. Their formation is a result of extra electron–positron or electron–electron correlations (which means that their contribution to the total annihilation spectrum should, in general, be smaller). The simplest of such states contains two holes and one excited electron. The corresponding amplitude in the lowest (first) order is shown in figure 4.

It is easy to see how these diagrams contribute to the right-hand side of equation (26). Thus, B1 times B1* (integrated over \mathbf{P}) becomes diagram Z7, B1 times the exchange analogue of B1* results in diagram Z8, while B2 times B2* gives diagram Z5. At the same time, B1 times B3*,

$$\sum_{vn} \frac{\langle n_1 n_2 | V | n \mu_1 \rangle \langle \varepsilon n | \delta | \mathbf{P} \rangle \langle \mathbf{P} | \delta | n_2 v \rangle \langle v \mu_1 | V | n_1 \varepsilon \rangle}{(\varepsilon - \varepsilon_{2\gamma} + \varepsilon_n)(\varepsilon - \varepsilon_v - \varepsilon_{\mu_1} + \varepsilon_{n_1})}, \quad (29)$$

does not lead to any Z_{eff} diagram after integration over \mathbf{P} . In fact, it does not lead to any valid diagrammatic expression at all. However, the matrix elements in equation (29) match those in equation (28). Using the energy conservation for the process in figure 4, $\varepsilon = \varepsilon_{2\gamma} + \varepsilon_{\mu_1} - \varepsilon_{n_1} - \varepsilon_{n_2}$, we see that the first energy denominator in (29) is equal to $\varepsilon_n + \varepsilon_{\mu_1} - \varepsilon_{n_1} - \varepsilon_{n_2}$, while the first energy denominator in (28) is equal to $-\varepsilon_n - \varepsilon_{\mu_1} + \varepsilon_{n_1} + \varepsilon_{n_2}$. Hence, the two expressions cancel term by term, as (28) is summed over the hole states n and (29) is summed over the electron and hole states v_1, n_1 and n_2 .

Note that this cancellation of the two anomalous contributions to the total annihilation rate, Z_{eff} , is exact. However, it occurs even before the integration over the momentum of the photons. This means that these contributions can be omitted when calculating the photon momentum distribution and gamma spectrum. In particular, diagram A5 in figure 2 can be ignored. A similar cancellation also takes place for other diagrams representing corrections to the annihilation vertex, in which the incident positron line is connected with the final-state hole by means of Coulomb interactions and electron–hole pairs. In all of these diagrams, annihilation occurs in the presence of one or more virtual electron–hole pairs.

In principle, the photon spectra corresponding to different final ionic states (e.g., those shown in figures 2 and 4) could be considered separately. In this case, the contributions (28) and (29) are not added together, and do not cancel each other. In practice, though, the total energy of the two photons or the final state of the ion is usually not observed. The shift of

the centre of the gamma line due to the difference in the total photon energy is negligible (as explained in section 2.2) and the cancellation described above does take place.

4. Evaluation of the diagrams

Let us consider a positron with momentum \mathbf{k} which collides with a closed-shell atom in the ground state, and annihilates, creating a hole in state n . The amplitude of this process is shown diagrammatically in figure 2. Let us denote it by $A_{n\mathbf{k}}(\mathbf{P})$. Omitting the QED factor $\pi r_0^2 c$ in equation (9), we write the photon energy spectrum in this process as

$$w_n(\epsilon) = \frac{1}{c} \int \int_{2|\epsilon|/c}^{\infty} |A_{n\mathbf{k}}(\mathbf{P})|^2 \frac{P \, dP \, d\Omega_{\mathbf{P}}}{(2\pi)^3}. \quad (30)$$

Integration over ϵ gives the contribution of hole n to the total annihilation rate

$$Z_{\text{eff}}(n) = \int w_n(\epsilon) \, d\epsilon = \int |A_{n\mathbf{k}}(\mathbf{P})|^2 \frac{d^3 P}{(2\pi)^3}. \quad (31)$$

4.1. Zeroth order

In the zeroth approximation, the amplitude $A_{n\mathbf{k}}(\mathbf{P})$ is given by diagram A0, figure 2,

$$A_{n\mathbf{k}}(\mathbf{P}) = \langle \mathbf{P} | \delta | n\mathbf{k} \rangle = \int e^{-i\mathbf{P}\cdot\mathbf{r}} \psi_n(\mathbf{r}) \varphi_{\mathbf{k}}(\mathbf{r}) \, d\mathbf{r}, \quad (32)$$

where

$$\psi_n(\mathbf{r}) = \frac{1}{r} P_{nl}(r) Y_{lm}(\Omega) \quad (33)$$

is the Hartree–Fock wavefunction of the occupied electron state in the orbital nl . The positron wavefunction is normalized to a plane wave, $\varphi_{\mathbf{k}}(\mathbf{r}) \sim e^{i\mathbf{k}\cdot\mathbf{r}}$, and can be written as a partial-wave expansion (Landau and Lifshitz 1982)

$$\varphi_{\mathbf{k}}(\mathbf{r}) = \frac{1}{r} \sqrt{\frac{\pi}{k}} \sum_{l_1=0}^{\infty} i^{l_1} \exp(i\delta_{l_1}) P_{\epsilon l_1}(r) P_{l_1}(\mathbf{k} \cdot \mathbf{r} / kr). \quad (34)$$

Here P_{l_1} is the Legendre polynomial, and $P_{\epsilon l_1}(r)$ is the positron radial wavefunction with energy $\epsilon = k^2/2$ and orbital angular momentum l_1 , normalized by

$$P_{\epsilon l_1}(r) \sim (\pi k)^{-1/2} \sin(kr - \frac{1}{2}\pi l_1 + \delta_{l_1}), \quad (35)$$

where δ_{l_1} is the phase shift. This normalization is to a δ -function of energy in Rydberg.

Using (33) and (34), and expanding $e^{-i\mathbf{P}\cdot\mathbf{r}}$ in spherical harmonics, we integrate over the angular variables in equations (32) and (30), and sum over the electronic magnetic quantum number m and spin. This gives the following expression for the spectrum of positron annihilation with an electron from orbital nl :

$$w_{nl}(\epsilon) = \frac{4}{ck} \sum_{\lambda, l_1} \int_{2|\epsilon|/c}^{\infty} |A_{n\epsilon}^{(\lambda)}(P)|^2 P \, dP, \quad (36)$$

where

$$A_{n\epsilon}^{(\lambda)}(P) = \sqrt{[\lambda][l][l_1]} \begin{pmatrix} \lambda & l & l_1 \\ 0 & 0 & 0 \end{pmatrix} \int_0^{\infty} j_{\lambda}(Pr) P_{nl}(r) P_{\epsilon l_1}(r) \, dr \equiv \langle P \| \delta_{\lambda} \| n\epsilon \rangle \quad (37)$$

is the *reduced* annihilation matrix element, in which $j_{\lambda}(z) = \sqrt{\frac{1}{2}\pi/z} J_{\lambda+1/2}(z)$ is the spherical Bessel function, λ is the angular momentum carried by the photons and the notation $[l] \equiv 2l+1$ is used. Equations (36) and (37) are similar to equation (III.6) of Farazdel and Cade (1977), for the angular correlation function in a positron bound state.

4.2. First order

The first-order correction A_1 , equation (22), is evaluated in a similar way, using (34) as the incident positron state ε . The wavefunctions of the intermediate electron and positron states μ and ν are written as

$$\psi_\mu(\mathbf{r}) = \frac{1}{r} P_{\varepsilon_\mu l_\mu}(r) Y_{l_\mu m_\mu}(\Omega), \quad \phi_\nu(\mathbf{r}) = \frac{1}{r} P_{\varepsilon_\nu l_\nu}(r) Y_{l_\nu m_\nu}(\Omega), \quad (38)$$

and the Coulomb interaction V is also expanded in the spherical harmonics.

When the zeroth- and first-order contributions are added together, the gamma spectrum is again given by equation (36), where the amplitude is now

$$A_{n\varepsilon}^{(\lambda)}(P) = \langle P \| \delta_\lambda \| n\varepsilon \rangle - \sum_{\mu, \nu} \frac{\langle P \| \delta_\lambda \| \mu\nu \rangle \langle \nu\mu \| V^{(\lambda)} \| n\varepsilon \rangle}{\varepsilon - \varepsilon_\nu - \varepsilon_\mu + \varepsilon_n}. \quad (39)$$

In the above expression

$$\langle \nu\mu \| V^{(\lambda)} \| n\varepsilon \rangle = \sum_{\lambda'} (-1)^{\lambda+\lambda'} \begin{Bmatrix} \lambda & l_1 & l \\ \lambda' & l_\mu & l_\nu \end{Bmatrix} \langle \nu\mu \| V_{\lambda'} \| n\varepsilon \rangle \quad (40)$$

is the reduced matrix element of the Coulomb interaction within the electron–positron pair with angular momentum λ ,

$$\langle \nu\mu \| V_{\lambda'} \| n\varepsilon \rangle = \sqrt{[l_\nu][l_\mu][l][l_1]} \begin{pmatrix} l_\nu & \lambda' & l_1 \\ 0 & 0 & 0 \end{pmatrix} \begin{pmatrix} l_\mu & \lambda' & l \\ 0 & 0 & 0 \end{pmatrix} R_{\nu\mu n\varepsilon}^{\lambda'}, \quad (41)$$

is the usual reduced Coulomb matrix element, and

$$R_{\nu\mu n\varepsilon}^{\lambda'} = \int \int P_{\varepsilon_\nu l_\nu}(r_2) P_{\varepsilon_\mu l_\mu}(r_1) \frac{r_1^{\lambda'}}{r_1^{\lambda'+1}} P_{nl}(r_1) P_{\varepsilon l_1}(r_2) dr_1 dr_2 \quad (42)$$

is the radial Coulomb integral. In the amplitude (39) the sum over μ and ν implies summation (integration) over the orbital angular momenta and energies of the intermediate electron and positron states.

5. Numerical calculations and results

In this section, we present and analyse the gamma spectra obtained by using the zeroth- and first-order terms in the amplitude, equations (36), (37) and (39), for the noble gas atoms.

5.1. Details of the calculations

The calculation starts by determining the electron wavefunctions of the ground-state atom in the Hartree–Fock approximation. Subsequently, sets of incident positron and intermediate electron and positron states in the field of the ground-state atom are generated.

In experiments, the gamma spectra of noble gases were measured with thermalized room-temperature positrons ($k_B T = 25$ meV). At such low energies only the positron s wave contributes significantly to the annihilation signal, higher partial waves being suppressed by the centrifugal barrier. The shape of the annihilation spectrum is not sensitive to the exact value of the positron energy (as long as it remains small), and we calculate the spectra for the positron momentum of $k = 0.05$ au, corresponding to the energy of $\varepsilon = 34$ meV ($\sim \frac{3}{2} k_B T$).

The sets of intermediate positron and electron states with orbital angular momenta $l = 0$ –8 were calculated on a uniform mesh in momentum space, starting with $k_0 = 0.1$ au, and increasing in steps of $\Delta k = 0.2$ au, over 59 continuous spectrum wavefunctions.

The electron and positron wavefunctions were used to compute annihilation and Coulomb matrix elements, and construct the annihilation amplitudes (39) for a range of momenta P . Using those, the gamma spectra for the valence and inner subshells were calculated from equation (36).

It is known that single-centre expansions of the annihilation amplitudes converge slowly with respect to the angular momenta of the electron and positron orbitals involved (Mitroy and Ryzhikh 1998, Mitroy *et al* 2002, Gribakin and Ludlow 2002). Thus, Gribakin and Ludlow (2002) showed that the increments in the annihilation rate upon increasing the maximal angular momentum from $l - 1$ to l , decrease asymptotically as $(l + \frac{1}{2})^{-2}$. In application to the annihilation spectra, this means that the quantity obtained by summing over all intermediate electron and positron states with l up to l_{\max} converges to the value for $l_{\max} = \infty$ as

$$w(\epsilon)^{l_{\max}} \simeq w(\epsilon)^{[\infty]} - \frac{A}{l_{\max} + \frac{1}{2}}, \quad (43)$$

where A is some constant⁷. We used this relation to obtain the values of $w(\epsilon) \equiv w(\epsilon)^{[\infty]}$ by linear extrapolation of $w(\epsilon)^{l_{\max}}$ from the last two points.

The total spectra are found by adding the contributions of the different subshells. They can be compared with experimental data. Annihilation rates obtained by integration of the spectra over ϵ provide information on the relative contributions of various subshells to the total Z_{eff} and show the importance of the correlation correction and extrapolation over l_{\max} .

5.2. Results for Ar

In this section, we examine in detail the results of the calculations for Ar, using it as an example. The next section will present a summary of the results for all noble gas atoms.

Figure 5 shows the annihilation gamma spectra for the four outer subshells in Ar. They were obtained from equations (36) and (39) by including the electron and positron intermediate states with orbital angular momenta up to l_{\max} in the first-order term, with $l_{\max} = 0-8$. Since the spectra are symmetric, $w(-\epsilon) = w(\epsilon)$, only the positive energies are shown. The 1s subshell is not included, as its contribution is small and does not affect the results for the total spectrum.

In the plots the lowest (thin solid) curve labelled $l_{\max} = 0$ corresponds to the zeroth-order result (for 3p and 2p), or is very close to it (for 3s and 2s), since the contribution of the intermediate states with the zero angular momentum is very small. For greater angular momenta the contributions of successive l decrease slowly, as expected. The spectra obtained by extrapolation to $l_{\max} \rightarrow \infty$ (thick solid curves) are noticeably larger than those obtained with $l_{\max} = 8$. For the two outer subshells, extrapolation increases the spectra by about 20% at small ϵ . Details of the extrapolation procedure are illustrated in figure 6. In agreement with equation (43), the dependence of $w^{l_{\max}}(\epsilon)$ on $(l_{\max} + \frac{1}{2})^{-1}$ is close to linear at large l_{\max} .

Figure 5 shows that the effect of electron-positron correlations described by the first-order correction is strongest for the 3p and 3s subshells which have small ionization potentials ($I_{3p} = 15.76$ eV, $I_{3s} = 29.24$ eV). The electrons in the inner shells are much more strongly bound ($I_{2p} = 249$ eV, $I_{3s} = 326$ eV). This makes it harder for the positron to perturb their motion, and reduces the effect of correlations. Nevertheless, the first-order correction leads to a noticeable increase of the annihilation signal for them as well. The larger binding energies also mean that 2s and 2p electrons move at greater speeds and have a broader momentum

⁷ The second term on the right-hand side of (43) is only the leading term, the next one being $\propto (l_{\max} + \frac{1}{2})^{-2}$, and keeping $\frac{1}{2}$ next to large l_{\max} is simply a matter of convenience.

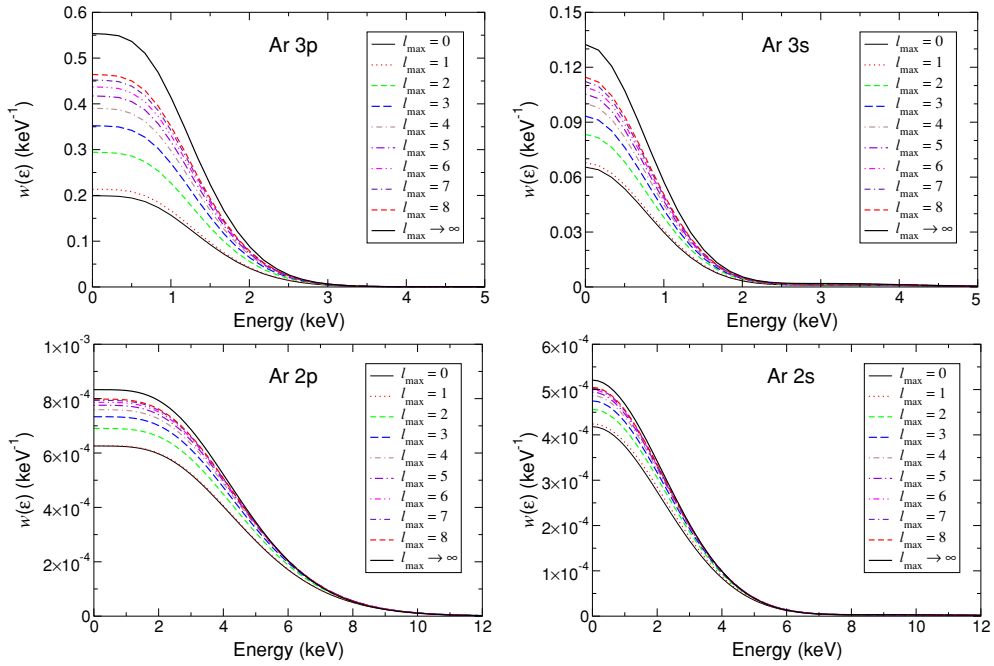


Figure 5. Gamma ray spectra $w_{nl}(\epsilon)$ for the positron annihilation on 3p, 3s, 2p and 2s subshells in Ar calculated using zeroth- and first-order diagrams. The graphs show how the result accumulates with the increase of the maximal orbital angular momentum l_{\max} of the intermediate electron and positron states in the first-order diagram. Thick solid curve is the result of extrapolation to $l_{\max} \rightarrow \infty$, equation (43).

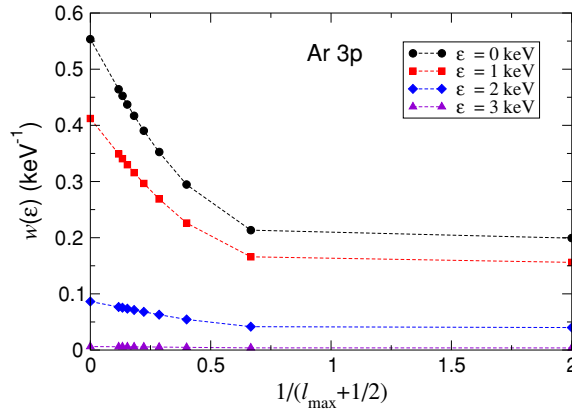


Figure 6. Extrapolation of the spectral density $w_{3p}(\epsilon)$ with respect to l_{\max} . Different symbols show the spectra calculated for $l_{\max} = 0-8$ and $l_{\max} \rightarrow \infty$, for different energies: full circles, $\epsilon = 0$ keV; squares, $\epsilon = 1$ keV; diamonds, $\epsilon = 2$ keV; triangles, $\epsilon = 3$ keV. The values at $(l_{\max} + \frac{1}{2})^{-1} = 0$ are obtained by linear extrapolation, equation (43), from the values for $l_{\max} = 7$ and 8.

distribution. As a result, their gamma spectra are wider, as seen in figure 5. Because of the repulsion from the nucleus, the positron wavefunction has a weaker overlap with the inner-shell electron orbitals, and their contribution to the positron–atom annihilation rate is much smaller than that of the valence shell.

Table 1. Full widths at half-maximum of the gamma spectra for Ar (in keV).

Subshell	Zeroth order	Zeroth + first order	
		$l_{\max} = 8$	$l_{\max} \rightarrow \infty$
2s	5.18	5.20	5.15
2p	9.42	9.29	9.18
3s	1.86	1.84	1.82
3p	2.89	2.75	2.71
Total	2.65	2.58	2.55

Table 2. Contribution of the outer and inner-shell electrons to Z_{eff} in Ar.

Subshell	Zeroth order	Zeroth + first order	
		$l_{\max} = 8$	$l_{\max} \rightarrow \infty$
2s	0.002 37	0.002 84	0.002 89
2p	0.006 21	0.007 77	0.008 01
3s	0.135 85	0.232 65	0.266 10
3p	0.605 62	1.340 68	1.578 87
Total	0.750 05	1.583 94	1.855 87

Tables 1 and 2 quantify the effect of the first-order correlation correction on the shapes of the gamma spectra and annihilation rates. Table 1 gives the full widths at half-maximum (FWHM) of the annihilation spectra for different orbitals. It shows that the first-order correction reduces the FWHM values of the spectra. This can be explained by noticing that in the first-order diagram (A1) the positron annihilates with an excited electron ‘pulled out’ of the atom. The wavefunction of such excited electron is less localized than the bound state wavefunction. The corresponding typical electron momenta are lower, making for smaller Doppler shifts and a narrower gamma spectrum.

The results shown in table 2 are the breakdown of the annihilation rate Z_{eff} for the 2s, 2p, 3s and 3p subshells. Partial Z_{eff} were obtained by integration of the corresponding spectral densities $w_{nl}(\epsilon)$, equation (31). According to the table, extrapolation over l_{\max} beyond $l_{\max} = 8$ increases the Z_{eff} values by about 15% for the 3s and 3p orbitals, and by 2–3% for the $n = 2$ orbitals. The final values show that adding the correlation correction more than doubles the Z_{eff} value for the $n = 3$ shell, compared with the zeroth-order calculation. It also increases the contributions of the 2s and 2p subshells, by 22% and 28%, respectively. Given their large binding energies, this is a remarkably strong correlation effect. In particular, it is much greater than the contribution of the $n = 2$ electrons to the positron–atom correlation potential, which can be estimated from their contribution to the dipole polarizability of Ar.

The size of the correlation effect for the inner-shell electrons can be compared with the *enhancement factor* for positron annihilation on hydrogen-like positive ions (Novikov *et al* 2004). This factor is defined as the ratio of Z_{eff} calculated with an accurate correlated wavefunction to the value obtained using a product of electron and positron densities $n_{\pm}(\mathbf{r})$: $Z_{\text{eff}} = \int n_{-}(\mathbf{r})n_{+}(\mathbf{r}) \mathbf{dr}$. The latter equation would be correct if the total wavefunction of the system was an uncorrelated product of the electron and positron wavefunctions (cf equation (14)). In the many-body theory approach, the enhancement factor can be defined as the ratio of Z_{eff} calculated from the expansion in figure 3 to the value obtained from the

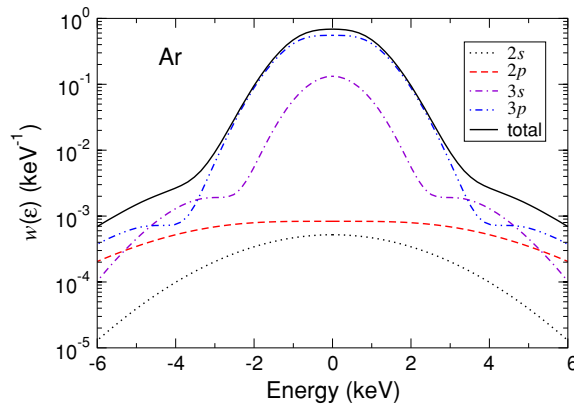


Figure 7. Gamma spectra for 2s, 2p, 3s and 3p subshells in Ar obtained in the zeroth + first-order calculation: \cdots , 2s; $---$, 2p; $-\cdot-$, 3s; $---$, 3p; $---$, total.

zeroth-order diagram Z0, equation (24) (Dzuba *et al* 1996, Gribakin and Ludlow 2004). This enhancement factor describes the effect of short-range electron–positron correlations (Dzuba *et al* 1996). For the annihilation of s-wave positrons on the valence electrons of noble gas atoms and hydrogen, it ranges from about 2.5 for Ne to 6 for Xe and H (Dzuba *et al* 1996, Gribakin and Ludlow 2004, Ludlow 2003). According to Novikov *et al* (2004), the enhancement factors for B^{4+} and F^{8+} are 1.41 and 1.20, while the electron ionization potentials in these systems are 340 and 1100 eV, respectively. The ionization potentials of the 2s and 2p subshells of Ar are similar to the first of these values, and the enhancement factors for Z_{eff} due to the first-order correlation correction in table 1 are of comparable magnitude, 1.22 (2s) and 1.28 (2p).

In spite of the large increase of Z_{eff} above the zeroth-order result, the final total in table 2 (1.86) is still much smaller than the experimental $Z_{\text{eff}} = 26.77 \pm 0.09$ obtained with room-temperature positrons (Coleman *et al* 1975). Of course, the large size of the first-order diagram means that higher order corrections are also important, especially for the valence and subvalence orbitals. The main contribution here comes from electron–positron ladder diagrams (e.g., A2 in figure 2). Another important effect is the distortion of the positron wavefunction by the positron–atom correlation potential (such as that shown by diagram A3). As mentioned in section 3.2, this strong nonperturbative effect can be accounted for by calculating the positron wavefunction from the Dyson equation. All-order summation of the ladder diagram series and the Dyson equation for the positron have been incorporated in the calculations of Z_{eff} (Gribakin and Ludlow 2004, Ludlow 2003), yielding good agreement with accurate calculations for hydrogen and experiment for the noble gases. We are currently applying a similar approach to the calculation of gamma spectra (Dunlop and Gribakin 2006).

Figure 7 shows our final gamma spectra for the 2s, 2p, 3s and 3p subshells. Addition of the partial spectra leads to a smoother, almost featureless total. The contributions of the inner shells are very small near the centre of the line. However, they noticeably push the wings up at $|\epsilon| > 4$ keV, and contribute to an overall non-Gaussian appearance of the spectrum. A similar effect of *core annihilation* is a common feature in ACAR and Doppler broadening spectra of positron annihilation in solids (see, e.g., Lynn *et al* (1977), Alatalo *et al* (1995, 1996), Asoka-Kumar *et al* (1996), Eshed *et al* (2002)).

Let us now compare the total gamma spectrum with experiment. In Iwata (1997a), parameters of a large number of gamma spectra for atomic and molecular species were

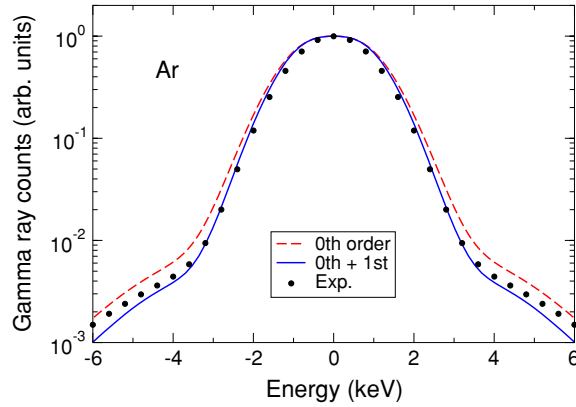


Figure 8. Comparison of the total spectrum for Ar with experimental data. All spectra have been normalized to unity at $\epsilon = 0$. Theory: ---, zeroth order; —, zeroth+first order. Experiment: ●, Iwata (1997), Iwata *et al* (1997a).

Table 3. γ -ray line-shape parameters from two-Gaussian fits (Iwata *et al* 1997a, Iwata 1997).

Atom	ΔE_1 (keV)	ΔE_2 (keV)	D
He	2.15	3.90	0.177
Ne	3.14	6.12	0.060
Ar	2.25	7.27	0.010
Kr	2.02	6.86	0.016
Xe	1.80	5.03	0.033

reported. The shapes of the spectra were determined by fitting the observed spectra with a two-Gaussian function

$$q(E) = \exp \left[- \left(\frac{E - E_0}{a\Delta E_1} \right)^2 \right] + D \exp \left[- \left(\frac{E - E_0}{a\Delta E_2} \right)^2 \right] \quad (44)$$

convolved with the detector response function (see also Iwata (1997)). In equation (44), $a = (4 \ln 2)^{-1/2}$, and the fitting parameters are the line centre E_0 , the FWHM of the two Gaussians, ΔE_1 and ΔE_2 , and the relative weight of the second Gaussian D . The line-shape parameters for the noble gas atoms are given in table 3.

In figure 8 we compare the experimental spectrum for Ar in the form (44), with the total spectra obtained in the zeroth- and zeroth+first-order approximations. For the purpose of comparison, all spectra are normalized to unity at zero energy shift ϵ . As discussed above, the inclusion of the first-order correction makes the spectrum narrower. It is also clear that the enhancement due to this contribution is stronger near the centre of the line and weaker in the wings. As a result, the wings of the zeroth+first-order spectrum in figure 8 appear to be suppressed. The experimental data clearly favour the curve which includes the correlation correction.

It must be said, though, that the overall *shape* of the gamma spectrum and, in particular, its FWHM value appear to be very robust. They are much less sensitive to the correlation correction than the absolute magnitude of the annihilation rate (as seen earlier in tables 1 and 2). The reason for such robustness of the shapes of the gamma spectra is that for slow positrons the momenta \mathbf{P} of the annihilating electron–positron pair are determined mainly by

Table 4. FWHM of the gamma spectra for the noble gas atoms (in keV).

Atom	Theory		Experiment ^a
	Zeroth order	Zeroth+first	
He	2.53	2.35	2.50 ± 0.03
Ne	3.82	3.63	3.36 ± 0.02
Ar	2.65	2.55	2.30 ± 0.02
Kr	2.38	2.30	2.09 ± 0.02
Xe	2.06	1.99	1.92 ± 0.02

^a Values obtained from Gaussian fits to the data (Van Reeth *et al* 1996, Iwata *et al* 1997a).

Table 5. Z_{eff} values for the noble gas atoms.

Atom	Theory		Experiment
	Zeroth	Zeroth+first	
He	0.688	1.395	3.94 ± 0.02 ^a
Ne	0.975	1.850	5.99 ± 0.08 ^a
Ar	0.750	1.856	26.77 ± 0.09 ^a
Kr	0.703	1.870	64.6 ± 0.08 ^a , 65.7 ± 0.3 ^b
Xe	0.645	1.887	400–450 ^b , 401 ± 20 ^c

^a Measured in the gas (Coleman *et al* 1975).

^b Measured in the gas, with small amounts of He or H₂ added to Xe to improve positron thermalization (Wright *et al* 1985).

^c Measured in the positron trap (Murphy and Surko 1990).

the momentum distribution of the bound electron. Such distribution is described well even at the Hartree–Fock level. This explains why Iwata *et al* (1997b) were able to obtain good fits of the experimental data with crude zeroth-order spectra, by adjusting the relative amounts of the outer- and inner-shell annihilation.

5.3. Summary of results for all noble gas atoms

Table 4 shows the FWHM values of the gamma spectra calculated using the zeroth- and zeroth+first-order approximations, as described in sections 5.1 and 5.2. For all atoms (except He), the spectrum contains the contributions of the two outermost shells, e.g., for Xe, annihilation on 4s, 4p, 4d, 5s and 5p electrons has been considered. For heavier noble gas atoms the contribution of inner-shell annihilation becomes more important (Iwata 1997b). However, it never exceeds few per cent, and has only a small effect on the FWHM values shown in table 4. We see that for all atoms except He, the addition of the correlation correction improves the agreement with experiment.

The changes in Z_{eff} (table 5) due to the first-order correction to the annihilation amplitude are more pronounced. The corresponding enhancement of the annihilation rate ranges from a factor of 1.9 in Ne to 2.9 in Xe. It is larger for heavier noble gas atoms, where the electrons are less strongly bound, making the correlation effect greater. Nevertheless, as in Ar, the final Z_{eff} values fall far short of experiment. Higher order corrections to the annihilation vertex ultimately increase it above the zeroth-order result by factors of 2.5 to 6, with a further increase coming from the distortion of the positron wavefunction by the positron–atom correlation potential (Dzuba *et al* 1996, Ludlow 2003). The latter effect becomes progressively

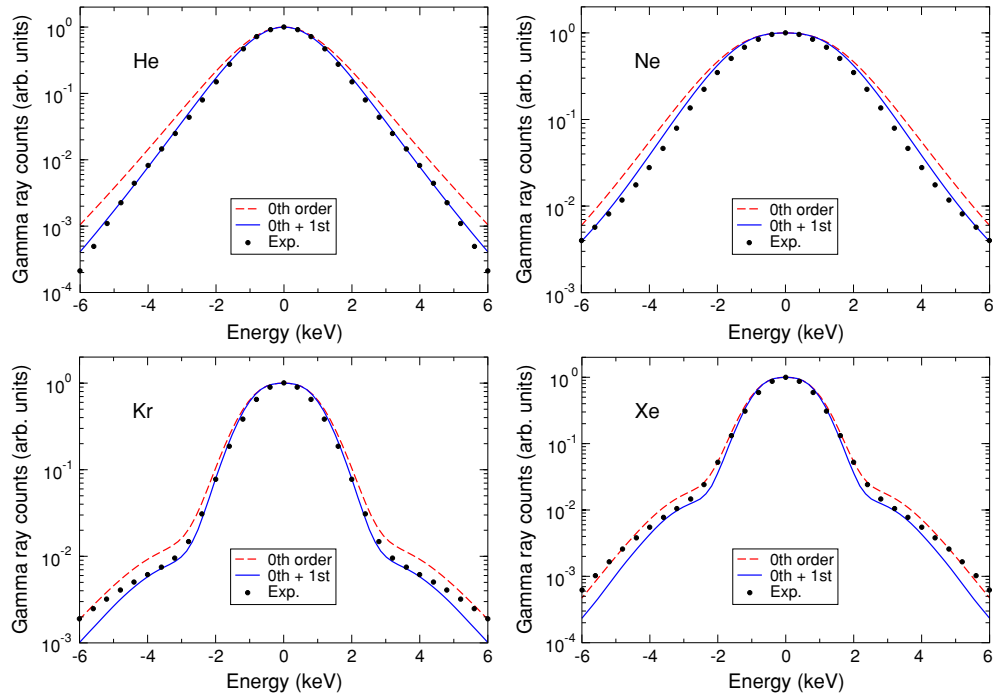


Figure 9. Comparison of the total gamma spectra for He, Ne, Kr and Xe with experiment. The spectra have been normalized to unity at $\epsilon = 0$. Theory: ---, zeroth order; —, zeroth+first order. Experiment: ●, Iwata (1997), Iwata *et al* (1997a).

stronger in Ar, Kr and Xe, due to the existence of virtual positron states with energies closer to zero (Dzuba *et al* 1996).

Finally, in figure 9 the gamma spectra calculated in the zeroth and zeroth+first-order approximations are compared with the two-Gaussian fits of the experimental data (Iwata 1997, Iwata *et al* 1997a). In all cases the inclusion of the vertex correction leads to better agreement with experiment. In particular, the relative contribution of the ‘shoulders’ associated with the inner-shell contributions in Kr and Xe is described more accurately. As in Ar, the enhancement of the annihilation rates due to correlations is greater for the outer np and ns electrons than for the inner $(n-1)d$, $(n-1)p$ and $(n-1)s$ subshells. When the total spectra are normalized to unity at $\epsilon = 0$, this results in suppression of the wings.

6. Summary and outlook

In this work, we have shown how a many-body perturbation series can be developed for the amplitude of positron–atom annihilation into photons with the total momentum \mathbf{P} . We have also shown how this series converts into a diagrammatic expansion of the annihilation rate Z_{eff} , upon integration over \mathbf{P} and summation over the final states.

Expressions for the zeroth and first-order diagrams in the annihilation amplitude have been derived, in terms of reduced δ -function and Coulomb matrix elements. These contributions have been evaluated numerically for the valence and inner subshells of the noble gas atoms. We have demonstrated the importance of extrapolation over the angular momentum of the intermediate electron and positron states. A comparison of the calculated and measured

gamma spectra has confirmed that inclusion of the correlation correction improves agreement with experiment. The correlation correction also leads to a sizeable enhancement of the annihilation rates, especially for the valence and subvalence orbitals.

The large role played by the first-order diagram means that higher order contributions must be considered. Thus, one needs to include vertex corrections containing the electron–positron ladder diagrams to all orders. One also needs to improve the incident positron wavefunction by taking into account the positron–atom correlation potential. So far, this programme has been realized in the calculations of positron–atom annihilation (Gribakin and Ludlow 2004, Ludlow 2003). Work is under way to implement this for the gamma spectra. This will allow us to obtain accurate gamma spectra for positron–atom annihilation. In particular, a much more accurate determination of the annihilation fraction of the inner-shell electrons in the noble gas atoms will be possible.

It is expected that our many-body theory work will provide further insights into the physical mechanisms which determine the shapes and intensities of the gamma spectra. We hope that this information, and possibly even some of the methods we are developing, will be useful for the studies of positron annihilation in more complex systems, such as molecules, clusters and condensed matter.

Acknowledgments

GG is grateful to J Ludlow, A V Korol, M G Kozlov and M Ya Amusia for the useful discussions concerning the many-body theory expansion of the annihilation amplitude. LJMD would like to thank DEL Northern Ireland for support in the form of a PhD studentship.

Appendix. Annihilation amplitude in the coordinate representation

Suppose the initial state of the system is that of a positron with momentum \mathbf{k} incident on a ground-state atom. The amplitude of finding the positron and one of the electrons at the same point and having a total momentum \mathbf{P} in an annihilation event which leaves the ion in the final state f is

$$A_{f\mathbf{k}}(\mathbf{P}) = \frac{1}{\sqrt{N}} \sum_{i=1}^N (-1)^i \int \Psi_f^*(\mathbf{r}_1, \dots, \mathbf{r}_{i-1}, \mathbf{r}_{i+1}, \dots, \mathbf{r}_N) e^{-i\mathbf{P}\cdot(\mathbf{r}+\mathbf{r}_i)/2} \times \delta(\mathbf{r} - \mathbf{r}_i) \Psi_{\mathbf{k}}(\mathbf{r}_1, \dots, \mathbf{r}_N, \mathbf{r}) d\mathbf{r}_1 \cdots d\mathbf{r}_N d\mathbf{r}. \quad (\text{A.1})$$

Here $\Psi_{\mathbf{k}}(\mathbf{r}_1, \mathbf{r}_2, \dots, \mathbf{r}_N, \mathbf{r})$ is the initial wavefunction of positron coordinate \mathbf{r} and N electron coordinates \mathbf{r}_i , and $\Psi_f(\mathbf{r}_1, \dots, \mathbf{r}_{N-1})$ is the wavefunction of the ion in the final state f . The initial state is normalized at large positron–atom separations according to $\Psi_{\mathbf{k}}(\mathbf{r}_1, \dots, \mathbf{r}_N, \mathbf{r}) \simeq \Phi_0(\mathbf{r}_1, \dots, \mathbf{r}_N) e^{i\mathbf{k}\cdot\mathbf{r}}$, where Φ_0 is the target ground-state wavefunction. Since the positron can annihilate with any target electron, the terms in the sum over i are antisymmetrized by the $(-1)^i$ factor. Formula (A.1) is analogous to equation (2) of Mitroy *et al* (2002).

To obtain the total annihilation rate, amplitude (A.1) must be squared and integrated over \mathbf{P} , and a sum over all final states of the ion should be taken:

$$Z_{\text{eff}} = \sum_f \int |A_{f\mathbf{k}}(\mathbf{P})|^2 \frac{d^3\mathbf{P}}{(2\pi)^3} = \int \sum_{i=1}^N \delta(\mathbf{r} - \mathbf{r}_i) |\Psi_{\mathbf{k}}(\mathbf{r}_1, \dots, \mathbf{r}_n, \mathbf{r})|^2 d\mathbf{r}_1 \cdots d\mathbf{r}_n d\mathbf{r}. \quad (\text{A.2})$$

In the lowest approximation, the initial-state wavefunction can be written as a product of the positron and target wavefunctions

$$\Psi_{\mathbf{k}}(\mathbf{r}_1, \dots, \mathbf{r}_N, \mathbf{r}) = \Phi_0(\mathbf{r}_1, \dots, \mathbf{r}_N)\varphi_{\mathbf{k}}(\mathbf{r}), \quad (\text{A.3})$$

where Φ_0 is the wavefunction of the target in the Hartree–Fock approximation (Slater determinant) and $\varphi_{\mathbf{k}}(\mathbf{r})$ is the incident positron wavefunction. Assuming that Ψ_f is also a Slater determinant in which a single-particle electron state n is missing, we obtain the annihilation amplitude

$$A_{n\mathbf{k}}(\mathbf{P}) = \int e^{-i\mathbf{P}\cdot\mathbf{r}}\psi_n(\mathbf{r})\varphi_{\mathbf{k}}(\mathbf{r}) \, d\mathbf{r}, \quad (\text{A.4})$$

which is identical to the zeroth-order expression (32).

References

- Alatalo M, Barbiellini B, Hakala M, Kauppinen H, Korhonen T, Puska M J, Saarinen A, Hautojärvi P and Nieminen R M 1996 *Phys. Rev. B* **54** 2397
- Alatalo M, Kauppinen H, Saarinen A, Puska M J, Mäkinen J, Hautojärvi P and Nieminen R M 1995 *Phys. Rev. B* **51** 4176
- Amusia M Ya and Cherepkov N A 1975 *Case Stud. At. Phys.* **5** 47
- Amusia M Ya, Cherepkov N A, Chernysheva L V and Shapiro S G 1976 *J. Phys. B: At. Mol. Phys.* **9** L531
- Arponen J and Pajanne E 1979 *J. Phys. F: Met. Phys.* **9** 2359
- Asoka-Kumar P, Alatalo M, Ghosh V J, Kruseman A C and Nielsen Band Lynn K G 1996 *Phys. Rev. Lett.* **77** 2097
- Berestetskii V B, Lifshitz E M and Pitaevskii L P 1982 *Quantum Electrodynamics* (Oxford: Pergamon)
- Carbotte J P 1967 *Phys. Rev.* **155** 197
- Chang L 1957 *Zh. Eksp. Teor. Fiz.* **33** 365
- Chang L 1958 *Sov. Phys.—JETP* **6** 281
- Coleman P G, Griffith T C, Heyland R G and Killeen T L 1975 *J. Phys. B: At. Mol. Phys.* **8** 1734
- Coleman P G, Rayner S, Jacobsen F M, Charlton M and West R N 1994 *J. Phys. B: At. Mol. Opt. Phys.* **27** 981
- Dunlop L J M and Gribakin G F 2006 *Phys. Rev. A* to be submitted
- Dzuba V A, Flambaum V V, Gribakin G F and King W A 1995 *Phys. Rev. A* **52** 4541
- Dzuba V A, Flambaum V V, Gribakin G F and King W A 1996 *J. Phys. B: At. Mol. Opt. Phys.* **29** 3151
- Dzuba V A, Flambaum V V, King W A, Miller B N and Sushkov O P 1993 *Phys. Scr. T* **46** 248
- Eshed A, Goktepe S, Koymen A R, Kim S, Chen W C, O’Kelly D J, Sterne P A and Weiss A H 2002 *Phys. Rev. Lett.* **89** 075503
- Farazdel A and Cade P E 1977 *J. Chem. Phys.* **66** 2612
- Ferrel R A 1956 *Rev. Mod. Phys.* **28** 308
- Fraser P A 1968 *Adv. At. Mol. Phys.* **4** 63
- Gribakin G F and King W A 1996 *Can. J. Phys.* **74** 449
- Gribakin G F and Ludlow J 2002 *J. Phys. B: At. Mol. Opt. Phys.* **35** 339
- Gribakin G F and Ludlow J 2004 *Phys. Rev. A* **70** 032720
- Iwata K 1997 *PhD Thesis* (San Diego, CA: Harcourt Brace Professional Publishing)
- Iwata K, Greaves R G and Surko C M 1997a *Phys. Rev. A* **55** 3586
- Iwata K, Gribakin G F, Greaves R G and Surko C M 1997b *Phys. Rev. Lett.* **79** 39
- Johnson W R, Buss D J and Carroll C O 1964 *Phys. Rev. A* **135** 1232
- Kahana S 1963 *Phys. Rev.* **129** 1622
- Landau L D and Lifshitz E M 1977 *Quantum Mechanics* (Oxford: Pergamon)
- Ludlow J 2003 *PhD Thesis* (Belfast: Queen’s University)
- Lynn K G, MacDonald J R, Boie R A, Feldman L C, Gabbe J D, Robbins M F, Bonderup E and Golovchenko J 1977 *Phys. Rev. Lett.* **38** 241
- McEachran R P, Stauffer A D and Campbell L E M 1980 *J. Phys. B: At. Mol. Phys.* **13** 1281
- Mitroy J, Bromley M W J and Ryzhikh G G 2002 *J. Phys. B: At. Mol. Opt. Phys.* **35** R81
- Mitroy J and Ryzhikh G G 1998 *J. Phys. B: At. Mol. Opt. Phys.* **32** 2831
- Murphy T J and Surko C M 1990 *J. Phys. B: At. Mol. Opt. Phys.* **23** L727

- Novikov S A, Bromley M W J and Mitroy J 2004 *Phys. Rev. A* **69** 052702
- Puska M J and Nieminen R M 1994 *Rev. Mod. Phys.* **66** 841
- Surko C M, Gribakin G F and Buckman S J 2005 *J. Phys. B: At. Mol. Opt. Phys.* **38** R57
- Tang S, Tinkle M D, Greaves R G and Surko C M 1992 *Phys. Rev. Lett.* **68** 3793
- Van Reeth P, Humberston J W, Iwata K and Surko C M 1996 *J. Phys. B: At. Mol. Opt. Phys.* **29** L465
- Wright G L, Charlton M, Griffith T C and Heyland G R 1985 *J. Phys. B: At. Mol. Phys.* **18** 4327